



Realization of broadband truly rainbow trapping in gradient-index metamaterials

JIE XU,^{1,2} SANSHUI XIAO,³ PANPAN HE,⁴ YAZHOU WANG,³ YUN SHEN,⁵ LUJUN HONG,^{5,6} YAMEI LUO,^{1,2,7} AND BING HE^{1,2,8}

¹School of Medical Information and Engineering, Southwest Medical University, Luzhou 646000, China

²Medical Engineering & Medical Informatics Integration and Transformational Medicine of Luzhou Key Laboratory, Luzhou 646000, China

³DTU Fotonik, Department of Photonics Engineering, Technical University of Denmark, DK-2800 Kgs. Lyngby, Denmark

⁴Department of Electronic Engineering, Luzhou Vocational and Technical College, Luzhou 646000, China

⁵Institute of Space Science and Technology, Nanchang University, Nanchang 330031, China

⁶ljhong@ncu.edu.cn

⁷luoluoyeran@126.com

⁸hebing_wu@163.com

Abstract: Unidirectionally propagating wave (UPW) such as surface magnetoplasmon (SMP) has been a research hotspot in the last decades. In the study of the UPW, metals are usually treated as perfect electric conductors (PECs). However, it was reported that the transverse resonance condition induced by the PEC wall(s) may significantly narrow up the complete one-way propagation (COWP) band. In this paper, ultra-broadband one-way waveguides are built by utilizing the epsilon-negative (ENG) metamaterial (MM) and/or the perfect magnetic conductor (PMC) boundary. In both cases, the total bandwidth of the COWP bands are efficiently enlarged by more than three times than the one in the original metal-dielectric-semiconductor-metal structure. Moreover, the one-way waveguides consisting of gradient-index metamaterial are proposed to achieve broadband truly rainbow trapping (TRT). In the full-wave simulations, clear broadband TRT without back reflection is observed in terahertz regime. Besides, giant electric field enhancement is achieved in a PMC-based one-way structure, and the amplitude of the electric field is enormously enhanced by five orders of magnitude. Our findings are beneficial for researches on broadband terahertz communication, energy harvesting and strong-field devices.

© 2022 Optica Publishing Group under the terms of the [Optica Open Access Publishing Agreement](#)

1. Introduction

Unidirectional or one-way electromagnetic (EM) modes attract more and more attentions in the past two decades [1–5] for its unique unidirectional propagation property which has extensive applications in optical communication. Similar to chiral edge states in quantum Hall effect, the one-way EM waves are immune to the backscattering, which has been observed in experiments at microwave frequency [6,7]. Engineering the band diagram of photonic crystals (PhCs) by introducing disorders is an efficient way to build one-way waveguide [2,8,9], and the cells of PhCs always consist of magneto-optical (MO) materials under a static magnetic field which is exploited to break the time-reversal symmetry of the system. Recently, numerous applications such as optical splitter [10–12], subwavelength focusing [13–15] and optical switch [16] were proposed based on the one-way waveguides. More recently, Tsakmakidis' group pointed out that the time-bandwidth (TB) limit which are believed to be a fundamental limit in engineering and physics, can be broken in a carefully designed one-way waveguide. In their work, Tsakmakidis et al. reported that the one-way surface magnetoplasmons (SMPs) propagating on the interface of silicon and InSb can be trapped and be localized in a subwavelength zero-dimensional cavity, and the TB limit was broken in such structure because of the nonreciprocity of such system [17].

According to the special theory of relativity, the speed of light must be a constant which means the light cannot be accelerated. On the contrary, slowing light or EM waves is much more easier. In the past decades, slowed or even trapped light was found in ultracold atomic gas [18], PhCs [19–22], grating structures [23,24], metamaterials (MMs) [25–27] and MO material heterostructures [28,29]. Among the slow-light structures, only a few of them can trap EM waves with different frequencies at different locations, namely rainbow trapping [30,31]. On the other hand, due to the coupling effect and reflection, most of the rainbow trapping systems cannot truly capture the EM waves [32,33]. The key point of truly rainbow trapping (TRT) is blocking the coupling between forward and backward propagating waves. Lately, we proposed a metal-semiconductor-semiconductor-metal structure, and by judiciously designing the thickness of the semiconductor layers, we achieved TRT in terahertz regime [34].

Nowadays, the study of the EM MMs with anomalous characteristics, without doubt, is one of the most interesting research directions. Novel MMs such as optical negative-index MMs [35–37], hyperbolic MMs [38–40], artificial magnetic conductor (AMC) MMs [41,42] and epsilon-negative (ENG) MMs [43–45] have been reported. Moreover, epsilon-near-zero (ENZ) MMs attract many attentions for its potential uses in studies of large nonlinearity [46], supercoupling [47], lens [48] and two dimensional materials [49]. Note that the ENZ MMs have been achieved using techniques such as effective medium theory [50], semiconductor doping [46] and applying a static electric field [51]. However, the study of stable ENG or ENZ MMs is still a research gap and in our opinion, reconfiguring the EM properties of MMs by cladding liquid crystal [52] may be a possible way to achieve such stable ENG or ENZ MMs. In this theoretical work, we consider the stable ENG and ENZ MMs in the study of ultra-broadband one-way waveguides and TRT. By utilizing the stable ENG/ENZ MMs and PMC wall(s), the complete one-way (unidirectional) propagation (COWP) band of the one-way configurations are significantly broadened. Moreover, we propose novel configurations consisting of gradient-index MMs in this work to achieve broadband TRT. Besides, we investigate the uses of the PMC boundary in the one-way waveguides and interestingly, giant electric field enhancement is observed in a PMC-based one-way waveguide which has an ultra-subwavelength terminal. All the theoretical analysis are verified by simulations utilizing finite element method.

2. Ultra-broadband one-way waveguide and broadband TRT

We first investigate the dispersion characteristics in a typical one-way terahertz structure and, as shown the inset of Fig. 1, the physical model consists of two layers of metal which can be treated as perfect electric conductor (PEC) in terahertz regime, and one layer of medium and one layer of semiconductor. We note here that, in this paper, the semiconductor is assumed to be N-type InSb. An external magnetic field (B_0) is applied on the InSb layer to break the time-reversal symmetry in the system. In our previous works, we have proved that the loss effect has almost no impact on the one-way property in such MO system [34,53]. Thus, we study the dispersion relation of SMPs in lossless condition in this work. The permittivity of InSb, as reported in many works [17,28,53], can be written as follow

$$\overset{\leftrightarrow}{\varepsilon} = \begin{bmatrix} \varepsilon_1 & 0 & i\varepsilon_2 \\ 0 & \varepsilon_3 & 0 \\ -i\varepsilon_2 & 0 & \varepsilon_1 \end{bmatrix} \quad (1)$$

with

$$\varepsilon_1 = \varepsilon_\infty \left(1 - \frac{\omega_p^2}{\omega^2 - \omega_c^2} \right), \varepsilon_2 = \varepsilon_\infty \frac{\omega_c \omega_p^2}{\omega (\omega^2 - \omega_c^2)}, \varepsilon_3 = \varepsilon_\infty \left(1 - \frac{\omega_p^2}{\omega^2} \right), \quad (2)$$

where ε_∞ , ω , ω_p , $\omega_c = eB_0/m^*$ (e and m^* represent the charge and the effective mass of an electron) are the high-frequency permittivity, the angular frequency, the plasma frequency and the electron cyclotron frequency, respectively. In this PEC-medium-semiconductor-PEC (EMSE) structure, the SMPs are sustained by the medium-InSb interface and due to the transverse resonance condition induced by the PEC walls, the dispersion relation of the SMPs should be distinctly changed compared to the one in the medium-semiconductor (MS) waveguide. The dispersion equation of the surface EM modes can be easily obtained by combining the Maxwell's equations and the boundary conditions, and according to our calculation, it has the following form [28]

$$\left(k^2 - \varepsilon_1 k_0^2\right) \tanh(\alpha d_2) + \frac{\varepsilon_1}{\varepsilon_m} \alpha_m \left[\alpha - \frac{\varepsilon_2}{\varepsilon_1} k \tanh(\alpha d_2)\right] \tanh(\alpha_m d_1) = 0 \quad (3)$$

where $\alpha = \sqrt{k^2 - \varepsilon_v k_0^2}$ ($\varepsilon_v = \varepsilon_1 - \varepsilon_2^2/\varepsilon_1$ is the Voigt permittivity), $\alpha_m = \sqrt{k^2 - \varepsilon_m k_0^2}$ (ε_m is the relative permittivity of medium) represent the transverse attenuation coefficients in the InSb layer and in the medium layer, respectively. d_1 and d_2 are the thicknesses of the medium and the InSb layers. Since we already have the dispersion equation of the SMPs, we can easily obtain the values of the asymptotic frequencies (AFs), one of the most important characteristics in the study of (nonreciprocal) unidirectional waveguides. Interestingly, when $k \rightarrow \pm\infty$, three asymptotic frequencies (AFs) are found in Eq. (3) and they are written as below

$$\omega_{sp}^{(1)} = \frac{1}{2} \left(\sqrt{\omega_c^2 + 4 \frac{\varepsilon_\infty}{\varepsilon_\infty + \varepsilon_m} \omega_p^2} - \omega_c \right), \omega_{sp}^{(2)} = \frac{1}{2} \left(\sqrt{\omega_c^2 + 4 \frac{\varepsilon_\infty}{\varepsilon_\infty + \varepsilon_m} \omega_p^2} + \omega_c \right), \omega_{sp}^{(3)} = \omega_c \quad (4)$$

To clearly show the special three AFs property, we plot the dispersion diagram of the EM modes in the EMSE waveguide in Fig. 1 for $\omega_c = 0.7\omega_p$, $d_1 = d_2 = 0.05\lambda_p$ ($\lambda_p = 2\pi c/\omega_p$) and $\varepsilon_m = 11.68$ (i.e. silicon). In this work, we will further explore the capability of the EMSE in building ultra-broadband one-way structures by utilizing MMs such as ENG MMs. In Fig. 1, the red solid lines, the black line and the dotted lines indicate the dispersion curves of SMPs and SMs [34] sustained by the semiconductor-metal interface and lowest-order normal modes in the light cone or bulk zones (the gray shaded regions), respectively. Note that the dispersion relation of the SMs and the normal modes can be easily derived from the Eq. (3) by changing the real and imaginary properties of α and α_m . Moreover, three horizontal arrows in Fig. 1 represent the values of three AFs. The yellow shaded region is the complete one-way propagation (COWP) band which is confined by ω_c ($= 0.7\omega_p$) and the cut-off frequency ($\omega_{cf} \approx 1.079\omega_p$, marked by the orange point) of the lowest-order normal modes. It is clear that in the $\omega < \omega_c$ region, the EM modes can propagate in both forward and backward directions since there are SMs with $v_g < 0$ and SMPs with $v_g > 0$. As a consequence, the bandwidth ($\Delta\omega \approx 0.379\omega_p$) of the COWP band is relatively small in this case. A possible way to widen the COWP band in such structure is to reduce or even eliminate the influences of SMPs in the $\omega < \omega_c$ region. In what follows, we will show that the ENG MMs could be used to achieve ultra-broadband one-way waveguide.

As shown in Fig. 2(a), the values of $\omega_{sp}^{(1)}$, $\omega_{sp}^{(2)}$, ω_c and ω_s ($\omega_s = \sqrt{\omega_c^2 + \omega_p^2}$) were plotted as a function of ε_m and ω_c . As a result, ω_c (the brown surface) is always smaller than ω_s (the green surface) while $\omega_{sp}^{(1)}$ (the purple surface) is invariably smaller than $\omega_{sp}^{(2)}$ (the blue surface). More interestingly, as shown in Fig. 2(b), $\omega_{sp}^{(1)} > \omega_c$ holds for $\varepsilon_m < 0$ as $\omega_c = 0.7$, implying that the dispersion curves of the SMPs may rise up in the case of $\varepsilon_m < 0$. Figure 2(c) illustrates the dispersion diagram of the EM modes in the EMSE model with $\varepsilon_m = -5$. Compared to Fig. 1, Fig. 2(c) demonstrates four AFs, two of which are $\omega_{sp}^{(1)}$ and $\omega_{sp}^{(2)}$ and they are significantly increased compared to the ones in Fig. 1. More importantly, the SMPs' dispersion curves rose up into the $\omega > \omega_c$ band, leading to three COWP bands (the yellow shaded regions) and one band gap

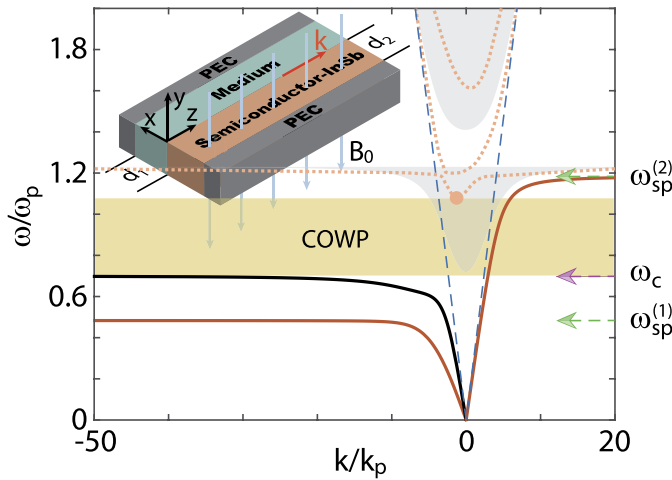


Fig. 1. The dispersion diagram of the PEC-Medium-Semiconductor-PEC (EMSE) model as $\omega_c = 0.7\omega_p$, $d_1 = d_2 = 0.05\lambda_p$ and $\epsilon_m = 11.68$. The red and black curves represent SMPs and SMs, respectively. The dotted lines are the low orders of normal modes in the medium (silicon, Si) and InSb layers, while the gray shaded zones and the blue dashed lines represent the bulk zones in semi-infinite InSb and the light lines of Si. The inset shows the schematic of the EMSE structure.

(the cyan region). The total bandwidth $\Delta\omega$ ($\approx 1.396\omega_p$) of the COWP regions in this case is about 3.7 times of the one in Fig. 1. In addition, the completely disappeared SMPs in the $0 < \omega < \omega_c$ band implies that the ENG MMs-based MO heterostructures have potential to excite pure one-way propagating SMs, which should have further uses in exploring on-chip nonreciprocal plasmonics [54].

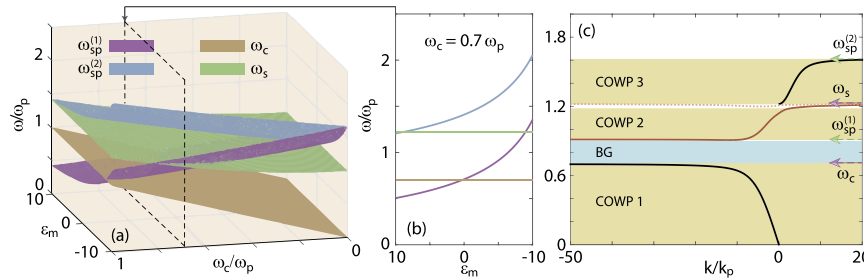


Fig. 2. $\omega_{sp}^{(1)}$, $\omega_{sp}^{(2)}$, ω_c and ω_s as a function of ϵ_m as (a) $0 < \omega_c < 1$ and (b) $\omega_c = 0.7\omega_p$. (c) The dispersion diagram of surface EM modes in Ultra-broadband one-way waveguide with $\epsilon_m = -5$. The other parameters are the same as in Fig. 1.

The emerged band gap (BG) in Fig. 2(c) is limited by ω_c and the cut-off frequency ($\approx \omega_{sp}^{(1)}$) of the dispersion branch of the SMPs (the red line), and excitingly, the BG falls in the COWP band in Fig. 1. On the other hand, it is clear that $\omega_{sp}^{(1)}$ gradually increases as ϵ_m decreases whereas ω_c is a constant. Therefore, the BG should be widen when decreasing ϵ_m . Accordingly, we believe that the truly rainbow trapping (TRT) can be achieved in novel heterostructures where the permittivity of the medium linearly decreases along the propagation direction (+z). To verify our conjecture, in Fig. 3(a), we first plot the values of $\delta\omega = \omega_c - \omega_{sp}^{(1)}$ as a function of ω_c for $\epsilon_m = 11.68$ and $\epsilon_m = -5$. The shaded area show the region in which $\delta\omega > 0$ for $\epsilon_m = 11.68$ and

$\delta\omega < 0$ for $\varepsilon_m = -5$. To achieve the TRT in the one-way waveguides consisting of medium with $-5 \leq \varepsilon_m \leq 11.68$, the external magnetic field should have an appropriate value and ω_c should fall in the shaded region, i.e. $0.5347 < \omega_c < 0.8578\omega_p$. As an example, we set $\omega_c = 0.7\omega_p$ and the broadband TRT theory are illustrated in Fig. 3(b), in which $\omega_{sp}^{(1)}$ (the red line), $\omega_{sp}^{(2)}$ (the pink line), ω_{cf} (the blue points) are plotted as a function of ε_m . The yellow regions and the cyan region represent the COWP bands and the BG, respectively. It is clear that, in Fig. 3(b), there is usually only one COWP band for $\varepsilon_m > 0$, and there are one or two (depending on ε_m) COWP bands and one BG for $\varepsilon_m < 0$. Note that with the decreases of ε_m , part of the COWP band gradually changes to a BG. The red point represents $\omega \approx 0.9126\omega_p$ which is the upper limit of the BG in the case of $\varepsilon_m = -5$. Meanwhile, the BG ($0.7\omega_p \leq \omega \leq 0.9126\omega_p$) falls in the COWP band in the case of $\varepsilon_m = 11.68$ (the black dashed line). Therefore, one can easily conclude that the EM wave with working frequency falls in $(0.7\omega_p, 0.9126\omega_p)$ band can unidirectionally propagating at the position of $\varepsilon_m = 11.68$ and be forbidden when $\varepsilon_m \leq -5$.

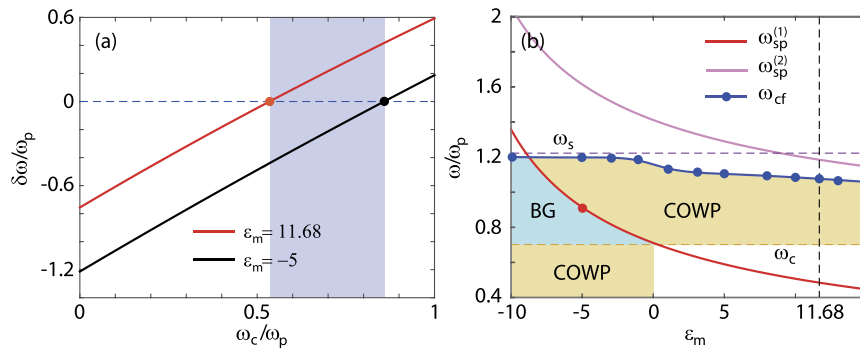


Fig. 3. (a) The relation between $\delta\omega = \omega_c - \omega_{sp}^{(1)}$ and ω_c in Si- and ENG-based EMSE waveguides for $0 < \omega_c < \omega_p$. (b) Three asymptotic frequencies, i.e. $\omega_{sp}^{(1)}$, $\omega_{sp}^{(2)}$ and ω_c , and the cut-off frequencies ω_{cf} as a function of ε_m .

Based on the results demonstrated in Fig. 3, we designed a novel EMSE waveguide (see the inset of Fig. 4(a)) which has four different EMSE parts, and the lengths of the four parts are respectively $L_1 = 80\mu\text{m}$, $L_2 = 40\mu\text{m}$, $L_3 = 160\mu\text{m}$ and $L_4 = 20\mu\text{m}$. Note that, in the simulations performed in this paper, the loss tangent of the ENG MMs was assumed to be 0.001 and the loss effects of InSb layer were considered by introducing the scattering frequency $v = 0.001\omega_p$, and the other parameters of InSb are $\varepsilon_\infty = 15.6$ and $\omega_p = 4\pi \times 10^{12} \text{ rad/s}$ [55]. Different with regular one-way waveguides, we assume the permittivities of the four parts of the EMSE structure are $\varepsilon_{m1} = 11.68$, $\varepsilon_{m2} = 11.68 - 6.68(z - L_1)/L_2$, $\varepsilon_{m3} = 5 - 10(z - (L_1 + L_2))/L_3$ and $\varepsilon_{m4} = -5$, respectively. It is worth noting that the gradient-index medium has been proposed in configurations such as sonic crystal [56] and photonic crystal [57]. The thicknesses of InSb and mediums are the same as in Fig. 3(b). Based on the above analysis, we know that $\omega_{sp}^{(1)} \approx 0.9126\omega_p$ for $\varepsilon_m = -5$, and, furthermore, the EM waves with $0.7\omega_p < \omega < 0.9126\omega_p$ should be trapped in our proposed waveguide shown in the inset of Fig. 4(a). Figure 4(b)–4(f) shows the electric field distributions in the simulations using finite element method (FEM) and the working frequencies are respectively $f = 0.72f_p$ ($f_p = 2 \text{ THz}$), $f = 0.78f_p$, $f = 0.84f_p$ and $f = 0.9f_p$. As a result, the EM waves with different frequencies are truly trapped in different place in the waveguide, which means the TRT are achieved in such structure. Here we emphasize that the regular trapped rainbow always suffers from the forward-backward coupling and that only the trapped rainbow without back reflection can be called truly trapped rainbow [32,34]. Compared to the regular rainbow trapping, we believe that the TRT is more suitable for designing high-performance optical

functional devices such as optical filters. Moreover, the EM waves in four simulations present the property of one-way propagation which is the most difference between regular rainbow trapping and one-way SMPs-based TRT. Figure 4(a) shows the amplitudes of the electric field on the medium-InSb interface and the phenomena of rainbow trapping and electric field enhancement were observed at the same time. Similarly, according to Fig. 3(b), it is capable of achieving the broadband TRT with the bandwidth $\Delta\omega_{\text{TRT}} \approx 0.4\omega_p$ in such gradient-index heterostructure. We emphasize that the above $\Delta\omega_{\text{TRT}}$ is more than three times wider than the one reported in our previous work [34]. It is also worth to note that one can see clearly the field discontinuity around $x = 200 \mu\text{m}$ in the TRT simulations (Fig. 4), which is arisen from the specific permittivity of the medium, i.e. $\epsilon_m = 0$. Note that epsilon-near-zero (ENZ) MMs have been widely studied in theory and experiments. In the next subsections, we will show that by using the PMC wall(s) and/or the ENZ MMs, the broadband TRT can be achieved as well.

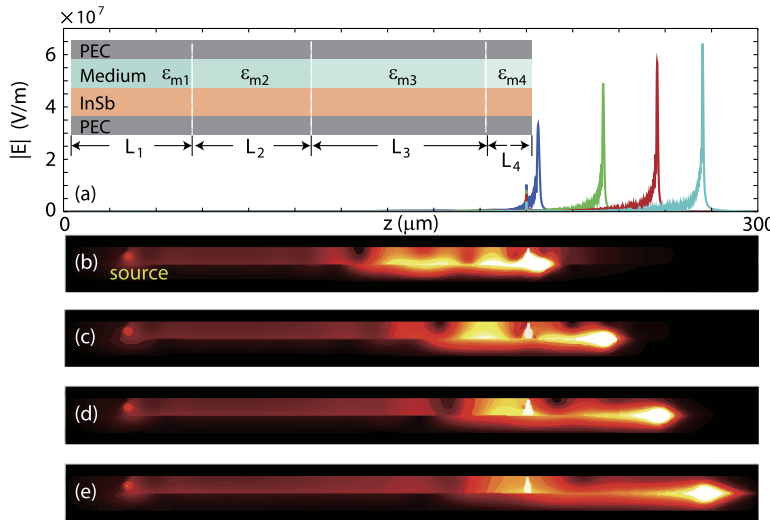


Fig. 4. (a) The electric field amplitude along the medium-InSb interface in the FEM simulations. The inset illustrates the designed rainbow-trapping EMSE configuration. (b)-(e) The simulated electric field distributions for $f = 0.72f_p$, $f = 0.78f_p$, $f = 0.84f_p$ and $f = 0.9f_p$. The source was placed at $z = 30 \mu\text{m}$ and $d_1/2$ above the medium-semiconductor interface. The electron scattering frequency are considered to be $\nu = 0.001\omega_p$ in the FEM simulations.

3. PMC-based one-way waveguides

Metal layers are usually treated as PEC walls in terahertz regime and based on our previous works, we found that the existence of the PEC walls may destroy the property of one-way propagation in ultra-subwavelength waveguides for the transverse resonance condition is introduced in such structures [28,34]. Here, we emphasize that the metal layers (PEC walls) can be replaced by PMC walls to break the limitation in the study of one-way EM modes in ultra-subwavelength MO heterostructures. As shown the left diagrams of Fig. 5, there are three ways using PMC wall(s), i.e. replacing the lower PEC wall, replacing the upper PEC wall and replacing all the PEC walls with PMC wall(s) in the EMSE configuration. Three new structures are respectively the PEC-medium-semiconductor-PMC (EMSM) structure, the PMC-medium-semiconductor-PEC (MMSE) structure and the PMC-medium-semiconductor-PMC (MMSM) structure. Similarly, the dispersion equations of the surface modes in these waveguides can be written as follow

$$\frac{\epsilon_2}{\epsilon_1}k + \frac{\alpha}{\tanh(\alpha d_2)} + \frac{\epsilon_v}{\epsilon_m}\alpha \tanh(\alpha_m d_1) = 0, \quad (\text{EMSM}) \quad (5)$$

$$\left(k^2 - \varepsilon_1 k_0^2\right) \tanh(\alpha d_2) + \frac{\varepsilon_1}{\varepsilon_m} \alpha_m \left[\alpha - \frac{\varepsilon_2}{\varepsilon_1} k \tanh(\alpha d_2)\right] \frac{1}{\tanh(\alpha_m d_1)} = 0, \quad (\text{MMSE}) \quad (6)$$

$$\frac{\varepsilon_2}{\varepsilon_1} k + \frac{\alpha}{\tanh(\alpha d_2)} + \frac{\varepsilon_v}{\varepsilon_m} \frac{\alpha}{\tanh(\alpha_m d_1)} = 0. \quad (\text{MMSM}) \quad (7)$$

We further plot the diagrams of the dispersion curves of the EM waves in these structures in Fig. 5 as $\omega_c = 0.7\omega_p$ and $d_1 = d_2 = 0.05\lambda_p$ ($\lambda_p = 150 \mu\text{m}$). Si and the ENG MM with $\varepsilon_m = -5$ are considered as two kinds of mediums in the EMSM waveguide (see Figs. 5(a,b)), in the MMSE waveguide (see Figs. 5(c,d)) and in the MMSM waveguide (see Figs. 5(e,f)). From Fig. 5, one can see that, for $\varepsilon_m = 11.68$, the numbers (N_{si}) of the COWP band (N_{cowl}) and the BG (N_{bg}) in the EMSM, MMSE and MMSM structures are $N_{si} = (N_{cowl}, N_{bg}) = (2, 1)$, $N_{si} = (2, 1)$ and $N_{si} = (2, 2)$, respectively. On the other hand, the corresponding numbers (N_{eng}) of the COWP

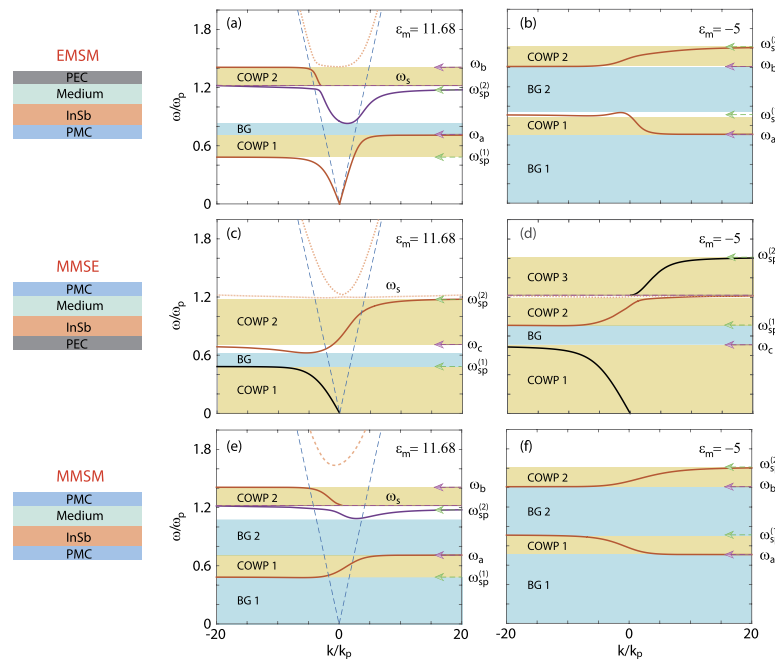


Fig. 5. The dispersion diagram of (a,b) the EMSM, (c,d) the MMSE and (e,f) the MMSM configurations. The mediums are considered being (a,c,e) silicon and (b,d,f) ENG MMs with $\varepsilon_m = -5$.

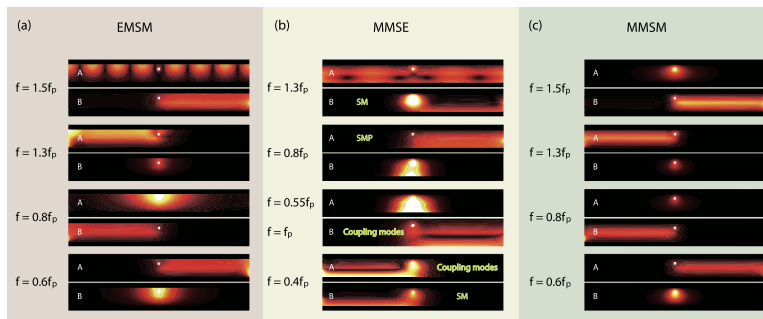


Fig. 6. The magnetic field distributions of the FEM simulations of (a) the EMSM, (b) the MMSE and (c) the MMSM structures. The other parameters are the same as in Fig. 5.

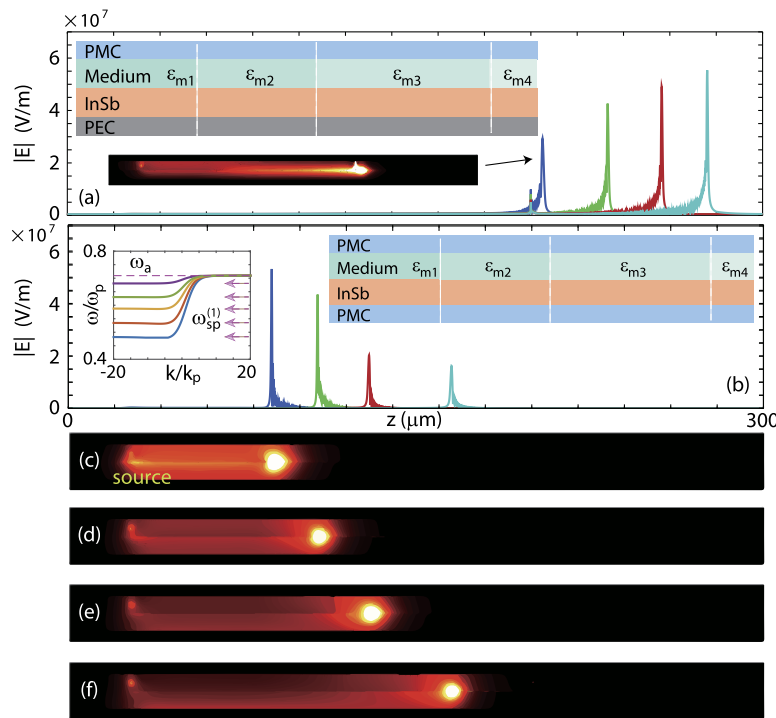


Fig. 7. Similar TRT as in Fig. 4 based on (a) the MMSE and (b) the MMSM configurations. The lower inset of (a) shows one of FEM simulation results of the trapped rainbow as $f = 0.72f_p$. The left inset of (b) represents the dispersion curves of the MMSM structure as $\epsilon_m = 11.68$ (blue line), $\epsilon_m = 8$ (red line), $\epsilon_m = 5$ (yellow line), $\epsilon_m = 3$ (green line) and $\epsilon_m = 1$ (purple line). The schematics of the MMSE and MMSM structures shown in (a) and (b) are almost the same with the one in Fig. 4(a) except for one or two layers PEC walls are replaced by PMC walls. (c)-(f) The electric field distributions in TRT based on the MMSM waveguide. Four working frequencies are $0.5f_p$, $0.55f_p$, $0.6f_p$ and $0.65f_p$, respectively. The source was placed at $z = 30$ μm and $d_1/2$ above the medium-semiconductor interface.

band and the BG in the cases of $\epsilon_m = -5$ are $N_{\text{eng}} = (2, 2)$, $N_{\text{eng}} = (3, 1)$ and $N_{\text{eng}} = (2, 2)$, respectively. Different with the EMSE structure, using the ENG MMs did not significantly enlarge the total bandwidth ($\Delta\omega$) of the COWP bands because the SMs disappeared in the EMSM and the MMSM structures. On the contrary, as shown in Fig. 5(c,d), the COWP band was obviously broadened in the ENG-based MMSE structure and $\Delta\omega \approx 1.4\omega_p$. That is to say, using the ENG MMs can build the ultra-broadband one-way waveguide in both the EMSE and the MMSE configurations. Moreover, as shown in Fig. 5(c), the SMs in the MMSE structure coupled with the SMPs and made a new COWP band ($\omega < \omega_{\text{sp}}^{(1)}$). We note that the EM modes falling in the new COWP band act like regular one-way SMs, which may have potential applications such as on-chip nonreciprocal terahertz communication [54,58]. In our opinion, using PMC wall to excite pure one-way SMs may be more practical than using ENG MMs proposed above (see Fig. 2(c)).

To verify the dispersion diagram illustrated in Fig. 5, we performed FEM simulations as working frequencies falling in the COWP bands or in the BGs, and the results are shown in Fig. 6. Symbols 'A' and 'B' represent the cases of $\epsilon_m = 11.68$ and $\epsilon_m = -5$, respectively. Note that, to clearly show the difference between SMs, SMPs and the coupling modes, the magnetic field distributions instead of the electric field distributions are chosen. In Fig. 6(b), the second

and the eighth pictures represent the SMs, and the sixth and the seventh pictures represent the coupling modes while the third picture represents a SMP. Interestingly, the coupling modes seem like propagate in both the medium-InSb and the metal-InSb interfaces. The other one-way propagating modes shown in Figs. 6(a) and 6(c) are SMPs, and all the results of the FEM simulations fit well with our theoretical analysis in lossless condition.

Similar with the EMSE waveguide, TRT without back reflections can be achieved in the MMSE and the MMSM waveguides. As shown in Fig. 7(a), we performed the full wave simulations in a MMSE waveguide (the upper inset) which has the same parameters with the one in Fig. 4(a) except for one of the PEC wall are replaced by a layer of PMC. The lower inset indicates the electric field distribution of one of the trapped rainbow which has the operating frequency $f = 0.72f_p$. We further performed the FEM simulations in a MMSM waveguide which is similar with the MMSE waveguide shown in Fig. 7(a) except for the lowest layer of metal was replaced by a layer of PMC. The working frequencies in this case were considered to be $f = 0.5f_p$, $f = 0.55f_p$, $f = 0.6f_p$ and $f = 0.65f_p$, respectively. The left inset of Fig. 7(b) shows the dispersion diagram in the MMSM structures as $\epsilon_m = 11.68$ (blue line), $\epsilon_m = 8$ (red line), $\epsilon_m = 5$ (yellow line), $\epsilon_m = 3$ (green line) and $\epsilon_m = 1$ (purple line), and four horizontal arrows represent the corresponding $\omega_{sp}^{(1)}$. It is clear that, in the MMSM structure, the COWP band limited by $\omega_{sp}^{(1)}$ and ω_a narrows down when ϵ_m decreases. Part of the COWP band gradually changed to a BG in the MMSM structure, in the same manner, implying the TRT. Figures 7(c)-(f) demonstrate the truly trapped rainbow with four working frequencies and the EM wave with the lower frequency was trapped at the location closer to the source. More interestingly, all the EM waves were trapped before a specific location, i.e. $z = 200\mu\text{m}$ (corresponding to $\epsilon_m = 0$), which implies that the TRT in a MMSM waveguide can be achieved by utilizing the epsilon-near-zero (ENZ) MMs instead of the ENG MMs.

4. Broadband TRT and ultra-subwavelength focusing

Besides the COWP 1 band, the COWP 2 band shown in Fig. 5(e) is also changed to a BG when ϵ_m changes from 11.68 to -5, which implies that similar TRT may be achieved in the COWP 2 band. Therefore, we performed the FEM simulations in a MMSM waveguide consisting of ENZ MMs in the COWP 2 band. The inset of Fig. 8(a) represents the ENZ-based MMSM waveguide which is similar with the one in Fig. 7(b) except for $\epsilon_{m1} = 11.68$, $\epsilon_{m2} = 11.68 - 6.68(z - L_1)/L_2$, $\epsilon_{m3} = 5 - 4.99(z - (L_1 + L_2))/L_3$ and $\epsilon_{m4} = 0.01$. Figures 8(b)-(e) shows the distributions of the simulated electric fields of the trapped waves. As one can see that the EM waves with four frequencies which are falling in the COWP 2 band are truly trapped in our designed MMSM waveguide since no reflections are observed in the opposite direction. We also emphasize that the EMSM model is not suitable to be used to achieve TRT in the COWP 2 band. As demonstrated in Figs. 8(f) and 8(g), with the decrease of ϵ_m , the cut-off frequencies (ω_{cf2} , marked by points in Fig. 8(f)) of the dispersion curves in the MMSM structure rise up and new BG emerges while the dispersion curves in the EMSM structure rise up in $k > 0$ region and unfortunately, there are SMPs in the whole region of $\omega < \omega_{sp}^{(2)}$. Thus, we conclude that the (broadband) TRT can be achieved in two different bands in the MMSM waveguides with the total bandwidth $\Delta\omega_{TRT} \approx 0.4\omega_p$.

Due to the nonattendance of the transverse resonance constraint, our proposed structures based on PMC also can be utilized in ultra-subwavelength focusing. As shown in the inset of Fig. 9(a), a MMSM waveguide consisting of one straight part and one tapered part was proposed to study the ultra-subwavelength focusing. The medium was set to be silicon (Si) and $\epsilon_m = 11.68$. The other parameters in the straight part of the MMSM structure are $L_1 = 150\mu\text{m}$, $L_2 = 200\mu\text{m}$ and $d_1 = d_2 = 0.05\lambda_p$ ($7.5\mu\text{m}$). The scale of right most end was set to be ultra-subwavelength and the thicknesses parameters are $d_1 = d_2 = 0.001\lambda_p$ ($0.15\mu\text{m}$). The lowest inset of Fig. 9(a) shows the simulated electric field distribution in the designed MMSM waveguide and the working frequency $f = 0.6f_p$ which, according to Fig. 5(e), is in the COWP band. Note that part of the

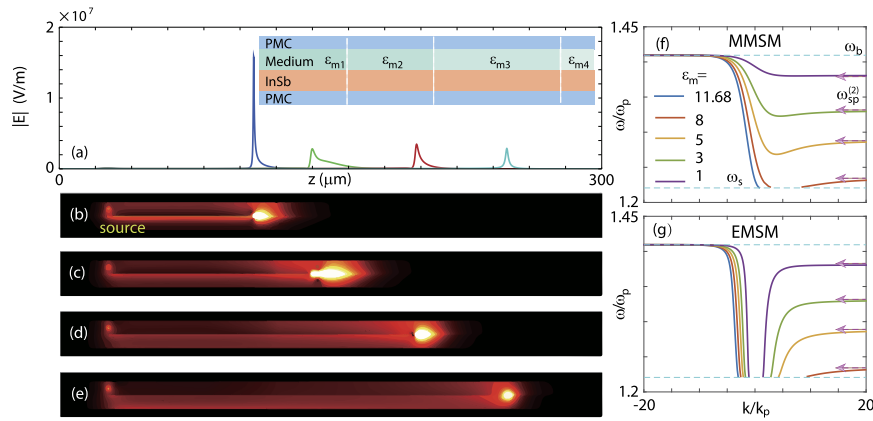


Fig. 8. Truly rainbow trapping in a MMSM waveguide consisting of ENZ MMs. (a) The electric field distributions along the interface of medium layer and InSb layer in the simulations. (b)-(e) The simulated electric field distributions as $f = 1.25f_p$, $f = 1.3f_p$, $f = 1.34f_p$ and $f = 1.38f_p$. The branches of the dispersion curves of SMPs in (f) the MMSM and (g) the EMSM waveguides when $\epsilon_m = 11.68$ (red line), $\epsilon_m = 8$ (blue line), $\epsilon_m = 5$ (green line), $\epsilon_m = 3$ (purple line) and $\epsilon_m = 1$ (black line). The external magnetic field is reversed and $\omega_c = -0.7\omega_p$. The source was placed at $z = 30 \mu\text{m}$ and $d_1/2$ above the medium-semiconductor interface.

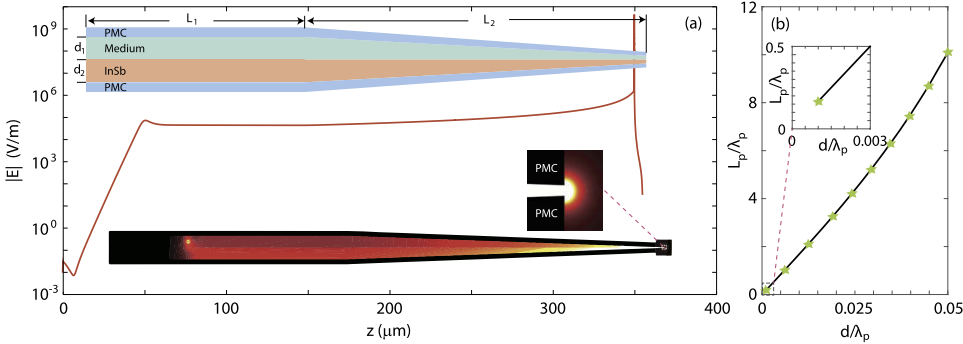


Fig. 9. (a) Ultra-subwavelength focusing based on the MMSM configuration. The upper inset shows the tapered MMSM waveguide designed for achieving ultra-subwavelength focusing. The lower inset shows the simulation result of the electric field focusing as $f = 0.6f_p$ and the right middle inset is the zoomed in picture around the terminal of the structure. The source was placed at $z = 50 \mu\text{m}$ and $d_1/2$ above the medium-semiconductor interface. The thicknesses of Si and InSb layers on the rightmost boundary of the structure are set to be equal and $d = 0.001\lambda_p$. The lengths of the uniform part and tapered part of the waveguide are respectively $L_1 = 150 \mu\text{m}$, $L_2 = 200 \mu\text{m}$. The other parameters are the same as in Fig. 4. (b) The propagation length (L_p) of SMPs in the MMSM waveguide when $d_1 = d_2 = d$ and $0 < d < 0.05\lambda_p$. The other parameters are $f = 0.6f_p$, $\omega_c = 0.7\omega_p$ and $v = 0.001\omega_p$.

tapered part of the MMSM waveguide was set in a air box (black box in the mostright end). Moreover, in our simulations, the excited EM wave unidirectionally propagated to the end surface and no reflection or interference was observed. Figure 9(a) demonstrates the amplitude of the electric field along the Si-InSb interface and, excitingly, extremely enhanced electric field were found near the end surface. According to the simulation, the max value of the enhancement factor

of the electric field is about 1.147×10^5 , which, as far as we know, has never been reported. To illustrate the loss impact on the electric field focusing, we calculated the propagation length (L_p) of the SMPs with $f = 0.6f_p$ for $d_1 = d_2 = d$ and $0.001\lambda_p \leq d \leq 0.05\lambda_p$. As a result, $L_p \approx 10.09\lambda_p$ ($\approx 1513.5\mu\text{m}$) as $d = 0.05\lambda_p$ and $L_p \approx 0.1669\lambda_p$ ($\approx 25.03\mu\text{m}$) as $d = 0.001\lambda_p$, which indicate that the corresponding EM wave propagates in the proposed waveguide with low loss.

5. Conclusion

In conclusion, we have investigated the potential uses of the epsilon-negative (ENG) metamaterials (MMs) and the perfect magnetic conductor (PMC) in one-way terahertz waveguides. In our theoretical analysis, ENG MMs and PMC walls can be used to design ultra-broadband one-way waveguide since the electromagnetic modes sustained on the semiconductor-metal interface (SMs) in the ENG- or PMC-based structures become unidirectional whereas the SMs in the regular one-way waveguides always suffer from the reverse propagating SMPs. Besides, we have proposed a novel way to achieve broadband ($\Delta\omega_{\text{TRT}} \approx 0.4\omega_p$, ω_p represents the plasma frequency) truly rainbow trapping (TRT) by utilizing the gradient-index MMs in the metal (PEC)-medium-semiconductor-PEC (EMSE) waveguide. We further explored the broadband TRT in three PMC-based structures, i.e. the PEC-medium-semiconductor-PMC (EMSM), the PMC-medium-semiconductor-PEC (MMSE) and the PMC-medium-semiconductor-PMC (MMSM) waveguides. As a result, broadband TRT was found in the gradient-index MMSE structure consisting of ENG MMs and in the gradient-index MMSM structure consisting of epsilon-near-zero (ENZ) MMs as well.

Owing to the robust one-way propagating property of the surface waves in the PMC-based waveguides, a straight-tapered MMSM waveguide was designed to study the ultra-subwavelength focusing at terahertz frequency. The thicknesses of the medium (silicon) and the semiconductor layers on the terminal were set to be the same and $d = 0.001\lambda_p$ (in this paper $\lambda_p = 150\mu\text{m}$). According to the full-wave simulation, a dramatically enhanced electric field was found around the terminal and the factor of the enhancement was about 1.147×10^5 . The loss effect was also considered in this case and the structure was proved to be low-loss. Our proposed ultra-broadband one-way waveguides, broadband TRT theory based on gradient-index MMs, and low-loss ultra-subwavelength focusing are promising for researches on nonlinear optics, ultra-strong electric-field devices, near-field imaging and broadband terahertz communication.

Funding. National Natural Science Foundation of China (61865009, 61927813); Department of Science and Technology of Sichuan Province (14JC0124, 14JC0153); Start-up funding of Southwest Medical University (20/00040186); Science and Technology Strategic Cooperation Programs of Luzhou Municipal People's Government and Southwest Medical University (2019LZXNYDJ18).

Disclosures. The authors declare that there are no conflicts of interest related to this article.

Data availability. No data were generated or analyzed in the presented research.

References

1. H. Takeda and S. John, "Compact optical one-way waveguide isolators for photonic-band-gap microchips," *Phys. Rev. A* **78**(2), 023804 (2008).
2. Z. Yu, G. Veronis, Z. Wang, and S. Fan, "One-way electromagnetic waveguide formed at the interface between a plasmonic metal under a static magnetic field and a photonic crystal," *Phys. Rev. Lett.* **100**(2), 023902 (2008).
3. X. Ao, Z. Lin, and C. Chan, "One-way edge mode in a magneto-optical honeycomb photonic crystal," *Phys. Rev. B* **80**(3), 033105 (2009).
4. S. A. Skirlo, L. Lu, and M. Soljačić, "Multimode one-way waveguides of large chern numbers," *Phys. Rev. Lett.* **113**(11), 113904 (2014).
5. Y. Yang, Y. F. Xu, T. Xu, H.-X. Wang, J.-H. Jiang, X. Hu, and Z. H. Hang, "Visualization of a Unidirectional Electromagnetic Waveguide Using Topological Photonic Crystals Made of Dielectric Materials," *Phys. Rev. Lett.* **120**(21), 217401 (2018).
6. R. E. Prange and S. M. Girvin, *The Quantum Hall effect* (Springer, 1987).
7. Z. Wang, Y. Chong, J. D. Joannopoulos, and M. Soljačić, "Observation of unidirectional backscattering-immune topological electromagnetic states," *Nature* **461**(7265), 772–775 (2009).

8. F. D. M. Haldane and S. Raghu, "Possible realization of directional optical waveguides in photonic crystals with broken time-reversal symmetry," *Phys. Rev. Lett.* **100**(1), 013904 (2008).
9. Z. Wang, Y. Chong, J. D. Joannopoulos, and M. Soljačić, "Reflection-free one-way edge modes in a gyromagnetic photonic crystal," *Phys. Rev. Lett.* **100**(1), 013905 (2008).
10. X. Zhang, W. Li, and X. Jiang, "Confined one-way mode at magnetic domain wall for broadband high-efficiency one-way waveguide, splitter and bender," *Appl. Phys. Lett.* **100**(4), 041108 (2012).
11. L. Hong, S. Xiao, X. Deng, R. Pu, and L. Shen, "High-efficiency tunable t-shaped beam splitter based on one-way waveguide," *J. Opt.* **20**(12), 125002 (2018).
12. C. He, X.-L. Chen, M.-H. Lu, X.-F. Li, W.-W. Wan, X.-S. Qian, R.-C. Yin, and Y.-F. Chen, "Tunable one-way cross-waveguide splitter based on gyromagnetic photonic crystal," *Appl. Phys. Lett.* **96**(11), 111111 (2010).
13. Q. Shen, L. Shen, W. Min, J. Xu, C. Wu, X. Deng, and S. Xiao, "Trapping a magnetic rainbow by using a one-way magnetostatic-like mode," *Opt. Mater. Express* **9**(11), 4399 (2019).
14. J. Xu, X. Deng, H. Zhang, C. Wu, M. Wubs, S. Xiao, and L. Shen, "Ultra-subwavelength focusing and giant magnetic-field enhancement in a low-loss one-way waveguide based on remanence," *J. Opt.* **22**(2), 025003 (2020).
15. Q. Shen, L. Hong, X. Deng, and L. Shen, "Completely stopping microwaves with extremely enhanced magnetic fields," *Sci. Rep.* **8**(1), 15811 (2018).
16. B. Hu, Q. J. Wang, and Y. Zhang, "Broadly tunable one-way terahertz plasmonic waveguide based on nonreciprocal surface magneto plasmons," *Opt. Lett.* **37**(11), 1895–1897 (2012).
17. K. Tsakmakidis, L. Shen, S. Schulz, X. Zheng, J. Upham, X. Deng, H. Altug, A. Vakakis, and R. Boyd, "Breaking lorentz reciprocity to overcome the time-bandwidth limit in physics and engineering," *Science* **356**(6344), 1260–1264 (2017).
18. L. V. Hau, S. E. Harris, Z. Dutton, and C. H. Behroozi, "Light speed reduction to 17 metres per second in an ultracold atomic gas," *Nature* **397**(6720), 594–598 (1999).
19. T. Baba, "Slow light in photonic crystals," *Nat. Photonics* **2**(8), 465–473 (2008).
20. S. Schulz, L. O'Faolain, D. M. Beggs, T. P. White, A. Melloni, and T. F. Krauss, "Dispersion engineered slow light in photonic crystals: a comparison," *J. Opt.* **12**(10), 104004 (2010).
21. H. Gersen, T. Karle, R. Engelen, W. Bogaerts, J. P. Korterik, N. Van Hulst, T. Krauss, and L. Kuipers, "Real-space observation of ultraslow light in photonic crystal waveguides," *Phys. Rev. Lett.* **94**(7), 073903 (2005).
22. H. Yoshimi, T. Yamaguchi, Y. Ota, Y. Arakawa, and S. Iwamoto, "Slow light waveguides in topological valley photonic crystals," *Opt. Lett.* **45**(9), 2648–2651 (2020).
23. Q. Gan, Z. Fu, Y. J. Ding, and F. J. Bartoli, "Ultrawide-Bandwidth Slow-Light System Based on THz Plasmonic Graded Metallic Grating Structures," *Phys. Rev. Lett.* **100**(25), 256803 (2008).
24. Q. Gan, Y. Gao, K. Wagner, D. Veenenov, Y. J. Ding, and F. J. Bartoli, "Experimental verification of the rainbow trapping effect in adiabatic plasmonic gratings," *Proc. Natl. Acad. Sci.* **108**(13), 5169–5173 (2011).
25. K. L. Tsakmakidis, A. D. Boardman, and O. Hess, "'trapped rainbow' storage of light in metamaterials," *Nature* **450**(7168), 397–401 (2007).
26. B. Zhang, H. Li, H. Xu, M. Zhao, C. Xiong, C. Liu, and K. Wu, "Absorption and slow-light analysis based on tunable plasmon-induced transparency in patterned graphene metamaterial," *Opt. Express* **27**(3), 3598–3608 (2019).
27. E. Gao, Z. Liu, H. Li, H. Xu, Z. Zhang, X. Zhang, X. Luo, C. Xiong, C. Liu, B. Zhang, and F. Zhou, "Dual dynamically tunable plasmon-induced transparency in h-type-graphene-based slow-light metamaterial," *J. Opt. Soc. Am. A* **36**(8), 1306–1311 (2019).
28. J. Xu, S. Xiao, C. Wu, H. Zhang, X. Deng, and L. Shen, "Broadband one-way propagation and rainbow trapping of terahertz radiations," *Opt. Express* **27**(8), 10659–10669 (2019).
29. Y. Yang, Y. Poo, R.-x. Wu, Y. Gu, and P. Chen, "Experimental demonstration of one-way slow wave in waveguide involving gyromagnetic photonic crystals," *Appl. Phys. Lett.* **102**(23), 231113 (2013).
30. Y. Yang, X. Shen, P. Zhao, H. C. Zhang, and T. J. Cui, "Trapping surface plasmon polaritons on ultrathin corrugated metallic strips in microwave frequencies," *Opt. Express* **23**(6), 7031–7037 (2015).
31. L. Liu, C. Yang, J. Yang, H. Xiang, and D. Han, "Spoof surface plasmon polaritons on ultrathin metal strips: from rectangular grooves to split-ring structures," *J. Opt. Soc. Am. B* **34**(6), 1130–1134 (2017).
32. K. Liu and S. He, "Truly trapped rainbow by utilizing nonreciprocal waveguides," *Sci. Rep.* **6**(1), 1–8 (2016).
33. S. He, Y. He, and Y. Jin, "Revealing the truth about 'trapped rainbow' storage of light in metamaterials," *Sci. Rep.* **2**(1), 583 (2012).
34. J. Xu, P. He, D. Feng, K. Yong, L. Hong, Y. Shen, and Y. Zhou, "Slow wave and truly rainbow trapping in a one-way terahertz waveguide," *Opt. Express* **29**(7), 11328–11341 (2021).
35. S. Xiao, V. P. Drachev, A. V. Kildishev, X. Ni, U. K. Chettiar, H.-K. Yuan, and V. M. Shalaev, "Loss-free and active optical negative-index metamaterials," *Nature* **466**(7307), 735–738 (2010).
36. V. M. Shalaev, "Optical negative-index metamaterials," *Nat. Photonics* **1**(1), 41–48 (2007).
37. J. Valentine, S. Zhang, T. Zentgraf, E. Ulin-Avila, D. A. Genov, G. Bartal, and X. Zhang, "Three-dimensional optical metamaterial with a negative refractive index," *Nature* **455**(7211), 376–379 (2008).
38. A. Poddubny, I. Iorsh, P. Belov, and Y. Kivshar, "Hyperbolic metamaterials," *Nat. Photonics* **7**(12), 948–957 (2013).
39. H. Hu, D. Ji, X. Zeng, K. Liu, and Q. Gan, "Rainbow trapping in hyperbolic metamaterial waveguide," *Sci. Rep.* **3**(1), 1249 (2013).
40. Y. Guo and Z. Jacob, "Thermal hyperbolic metamaterials," *Opt. Express* **21**(12), 15014 (2013).

41. A. Monti, L. Scorrano, S. Tricarico, F. Bilotti, A. Toscano, and L. Vigni, "Achieving PMC boundary conditions through metamaterials," *COMPEL: The Int. J. for Comput. Math. Electr. Eng.* **32**(6), 1876–1890 (2013).
42. A. Erentok, P. Luljak, and R. Ziolkowski, "Characterization of a volumetric metamaterial realization of an artificial magnetic conductor for antenna applications," *IEEE Trans. Antennas Propag.* **53**(1), 160–172 (2005).
43. M. Moniruzzaman, M. T. Islam, M. Tarikul Islam, M. E. Chowdhury, H. Rmili, and M. Samsuzzaman, "Cross coupled interlinked split ring resonator based epsilon negative metamaterial with high effective medium ratio for multiband satellite and radar communications," *Results Phys.* **18**, 103296 (2020).
44. P. Dawar and A. De, "Bandwidth enhancement of rmpa using eng metamaterials at thz," in *2013 4th International Conference on Computer and Communication Technology (ICCCT)*, (IEEE, 2013), pp. 11–16.
45. R. Kumari, P. N. Patel, and R. Yadav, "An ENG resonator-based microwave sensor for the characterization of aqueous glucose," *J. Phys. D: Appl. Phys.* **51**(7), 075601 (2018).
46. M. Z. Alam, I. De Leon, and R. W. Boyd, "Large optical nonlinearity of indium tin oxide in its epsilon-near-zero region," *Science* **352**(6287), 795–797 (2016).
47. B. Edwards, A. Alù, M. E. Young, M. Silveirinha, and N. Engheta, "Experimental Verification of Epsilon-Near-Zero Metamaterial Coupling and Energy Squeezing Using a Microwave Waveguide," *Phys. Rev. Lett.* **100**(3), 033903 (2008).
48. V. Torres, V. Pacheco-Peña, P. Rodríguez-Ulibarri, M. Navarro-Cía, M. Beruete, M. Sorolla, and N. Engheta, "Terahertz epsilon-near-zero graded-index lens," *Opt. Express* **21**(7), 9156 (2013).
49. S. Biswas, W. S. Whitney, M. Y. Grajower, K. Watanabe, T. Taniguchi, H. A. Bechtel, G. R. Rossman, and H. A. Atwater, "Tunable intraband optical conductivity and polarization-dependent epsilon-near-zero behavior in black phosphorus," *Sci. Adv.* **7**(2), eabd4623 (2021).
50. J. C. Vap, M. A. Marciak, M. Moran, and L. Johnson, "Examining epsilon near zero structures through effective medium theory and optical thin film analysis," in *Polarization: Measurement, Analysis, and Remote Sensing X*, vol. 8364 D. B. Chenault and D. H. Goldstein, eds., International Society for Optics and Photonics (SPIE, 2012), pp. 229–236.
51. E. Feigenbaum, K. Diest, and H. A. Atwater, "Unity-Order Index Change in Transparent Conducting Oxides at Visible Frequencies," *Nano Lett.* **10**(6), 2111–2116 (2010).
52. D. H. Werner, D.-H. Kwon, I.-C. Khoo, A. V. Kildishev, and V. M. Shalaev, "Liquid crystal clad near-infrared metamaterials with tunable negative-zero-positive refractive indices," *Opt. Express* **15**(6), 3342 (2007).
53. L. Shen, J. Xu, Y. You, K. Yuan, and X. Deng, "One-way electromagnetic mode guided by the mechanism of total internal reflection," *IEEE Photonics Technol. Lett.* **30**(2), 133–136 (2018).
54. Y. Liang, S. Pakniyat, Y. Xiang, J. Chen, F. Shi, G. W. Hanson, and C. Cen, "Tunable unidirectional surface plasmon polaritons at the interface between gyrotropic and isotropic conductors," *Optica* **8**(7), 952 (2021).
55. T. H. Isaac, W. L. Barnes, and E. Hendry, "Determining the terahertz optical properties of subwavelength films using semiconductor surface plasmons," *Appl. Phys. Lett.* **93**(24), 241115 (2008).
56. A. Climente, D. Torrent, and J. Sánchez-Dehesa, "Sound focusing by gradient index sonic lenses," *Appl. Phys. Lett.* **97**(10), 104103 (2010).
57. E. Centeno, D. Cassagne, and J.-P. Albert, "Mirage and superbending effect in two-dimensional graded photonic crystals," *Phys. Rev. B* **73**(23), 235119 (2006).
58. S. A. H. Gangaraj and F. Monticone, "Do truly unidirectional surface plasmon-polaritons exist?" *Optica* **6**(9), 1158–1165 (2019).